*A Study on Low Resolution Androgenic Hair Patterns for Criminal and Victim Identification

†Han Su and ‡Adams Wai Kin Kong, *Member, IEEE*

***Abstract*—Identifying criminals and victims in images (e.g., child pornography and masked gunmen) can be a challenging task, especially when neither their faces nor tattoos are observable. Skin mark patterns and blood vessel patterns are recently proposed to address this problem. However, they are invisible in low resolution images and dense androgenic hair can cover them completely. Medical research results have implied that androgenic hair patterns are a stable biometric trait and have potential to overcome the weaknesses of skin mark patterns and blood vessel patterns. To the best knowledge of the authors, no one studied androgenic hair patterns for criminal and victim identification before. This paper aims to study matching performance of androgenic hair patterns in low resolution images. An algorithm designed for this study uses Gabor filters to compute orientation fields of androgenic hair patterns, histograms on a dynamic grid system to describe their local orientation fields and the blockwise Chi-square distance to measure the dissimilarity between two patterns. 4,552 images from 283 different legs with resolutions of 25, 18.75, 12.5 and 6.25 dpi were examined. The experimental results indicate that androgenic hair patterns even in low resolution images are an effective biometric trait and the proposed Gabor orientation histograms are comparable with other well-known texture recognition methods, including local binary patterns, local Gabor binary patterns and histograms of oriented gradients.**

***Index Terms*—Hair pattern identification, criminal and victim identification, soft biometrics, skin marks**

I. Introduction

IDENTIFYING CRIMINALS and victims is always an important task in police investigation and forensic evaluation. Fingermarks, blood samples, DNA, dental records, tattoos, face images and face sketches are used regularly by law enforcement agents all around the world. However, they cannot handle the cases, where only images describing crime-scene specimens are available [59], but neither faces nor tattoos[§] are observable [6]. These cases include but not limited to child pornography, violent protests (e.g., the Rome and the London riots in 2011), masked gunmen and terrorist attacks, where criminals always cover or hide their faces and tattoos to avoid identification. Because of the recent advances in imaging technology and the popularity of digital cameras, images with criminals and victims have been increasing significantly.

To show the seriousness of the problem, we list some statistics about child sexual offenses. The U.S. Customs Service estimated that around 100,000 websites involve with child pornography [2]. From 2002 to 2008 in Canada alone, approximately 30,000 child pornography cases were reported [3]. The U.S. Bureau of Justice Statistics concluded that the low prosecution rate of child sex exploitation offenders was mainly due to inadmissible or weak evidence [1]. Though the U.S. Bureau of Justice Statistics defined neither inadmissible evidence nor weak evidence clearly, our forensic partners in two countries showed many child pornographic images and videos, which have only non-facial body sites of paedophiles and victims to the last author.

In addition to child sexual offenders, terrorists also make use of this identification difficulty. It is worth mentioning that tattoos are prohibited in extreme Islamic terrorist groups [4]. Once they wear face masks, there is currently no way to identify them. Numerous masked terrorist images are available on the Internet [50-57, 64]. Some masked terrorists even accept interviews from media.

Though neither faces nor tattoos are observable in these images describing crime-scene specimen, other body sites are often apparent. In child pornography cases, we likely obtain close up images with backs, chests and thighs of criminals or victims and in masked gunmen, violent protest and terrorist attack cases, we likely obtain images with arms and legs of criminals since they often wear T-shirts, short sleeve shirts and shorts, in particular in summer and hot climate regions. Some of these images can be found in [40-57, 64]. To address this challenging identification problem, blood vessel patterns and skin mark patterns are proposed recently [5, 13-14]. Blood vessel patterns are universal and are considered stable over a long period of time. Traditionally, near infrared imaging systems are used to capture blood vessel patterns. Methods are

Manuscript received March 2013. This work was supported in part by the Ministry of Education, Singapore.

Han Su is with College of Computer Science, Sichuan Normal University, 1819 Chenglong Road, Chengdu, Sichuan, China, 610101 and School of Computer Engineering, Nanyang Technological University, Block N4, Nanyang Avenue, Singapore 639798.

A.W.K. Kong is with School of Computer Engineering, Nanyang Technological University, Block N4, Nanyang Avenue, Singapore 639798 (phone: (65) 6513 8041; e-mail: adamskong@ntu.edu.sg).

*In different research communities, the word identification can have different meanings. In this paper, identification is a well-defined term in the biometric community [37]. It means one-to-many matching.

† All her work was done at the Nanyang Technological University.

‡ Correspondence author.

§ Note that tattoos may not be distinctive enough and different persons can have the same tattoo.

developed recently to visualize blood vessel patterns hidden in color images captured by consumer digital cameras [5, 14]. However, their visibility depends on image quality and physiological factors such as the thickness of the subcutaneous fat layer in the skin and its pigmentation level. Skin marks, occurring on the skin surface, are more easily observable than blood vessels. Skin mark patterns and blood vessel patterns both require high resolution images and dense androgenic hair can cover them completely. New biometric traits have thus to be developed.

Medical research results have indicated that androgenic hair patterns can be used as a biometric trait. There are no additional follicles naturally formed after birth in human beings [8]. All androgenic hairs manifest a cycle. When one hair drops, another new hair grows at the same follicle [7]. They are two different hair shafts, but appear at the same location. Androgenic hair cycle is long. A leg hair cycle can be up to one year [9]. Within this long period of time, we can find the same hair shaft. There are seasonal changes in androgenic hair growth [62]. A study showed that thigh hair grows faster in summer than in winter [63]. However, hair follicles have their own rhythm and their cycles are asynchronous, except in groups of three follicles called Demeijère [10, 58]. This implies that human hair does not fall out at the same time and we can always find some corresponding androgenic hairs for matching. The vellus-to-terminal hair follicle switch is irreversible. Even if men are castrated, their beards would not return to prepubertal level [11-12]. Only around 10% androgenic hair follicles exit permanently from cycling. Others cycle throughout the entire lifespan to produce hair [7]. Figs. 1(a) and (b) show two skin images from the same leg collected in August 2009 and October 2008 respectively. The color circles in Figs. 1(a) and (b) indicate the partial corresponding androgenic hair follicles. From this small area, we can find more than 40 corresponding androgenic hair follicles. The remaining images in Fig. 1 show four image pairs collected in different time periods. As with Figs. 1(a) and (b), a lot of corresponding androgenic hair follicles can be identified. However, androgenic hair follicles are only observable in high resolution images. This paper studies matching performance of androgenic hair patterns in low resolution images as an alternative biometric trait for criminal and victim identification. Fig. 2 shows four male legs with distinctive androgenic hair patterns. As with other biometric traits, including face and fingerprint, androgenic hair can be modified (e.g. laser hair removal). This paper does not consider modification of androgenic hair.

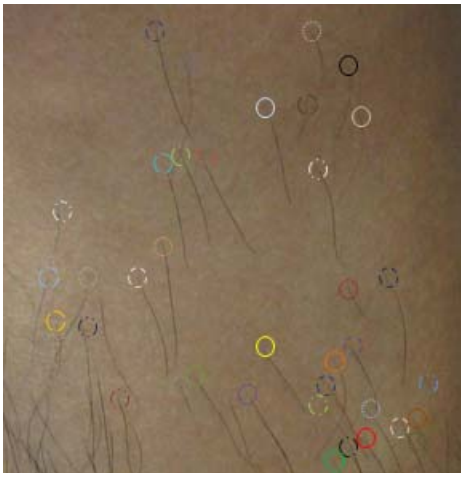

(a) was collected in August 2009.

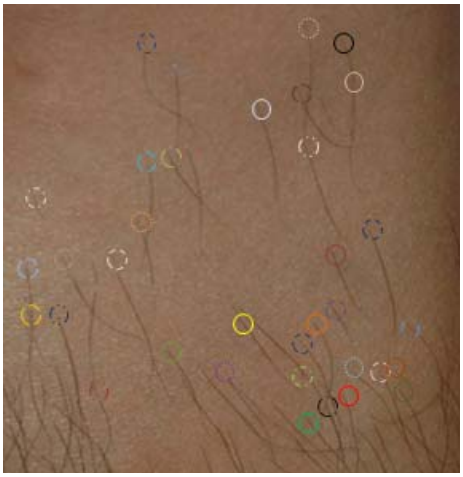

(b) was collected in October 2008.

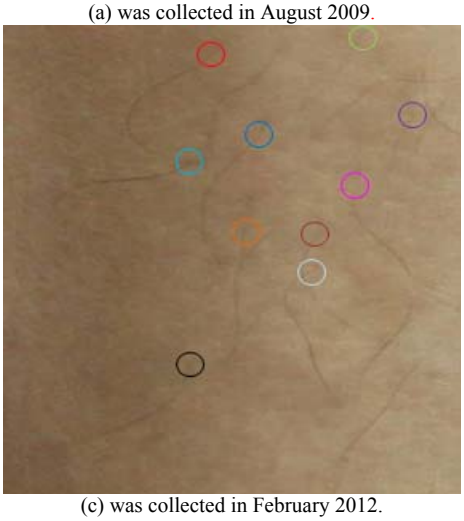

(c) was collected in February 2012.

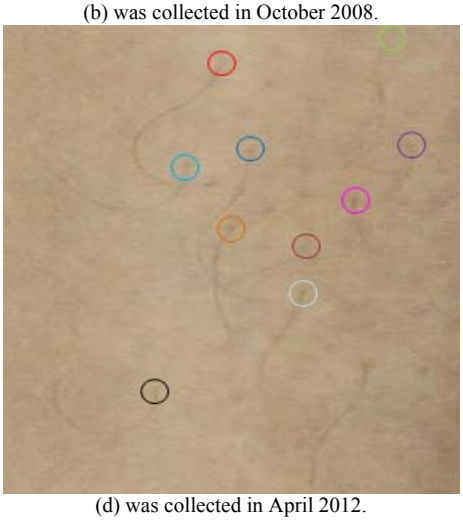

(d) was collected in April 2012.

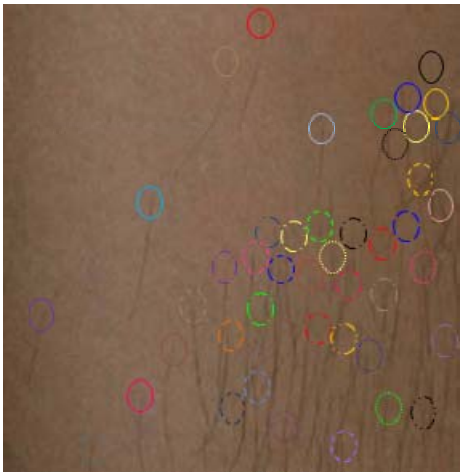

(e) was collected in October 2008.

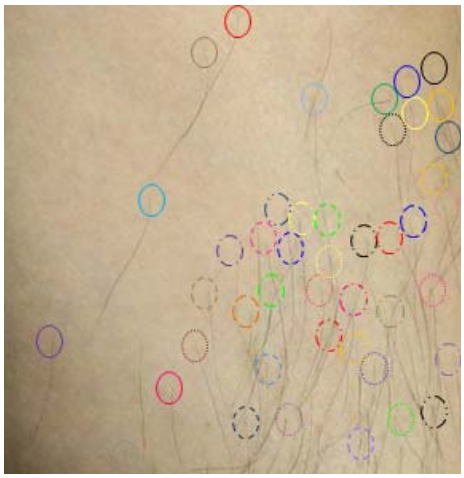

(f) was collected in February 2012.

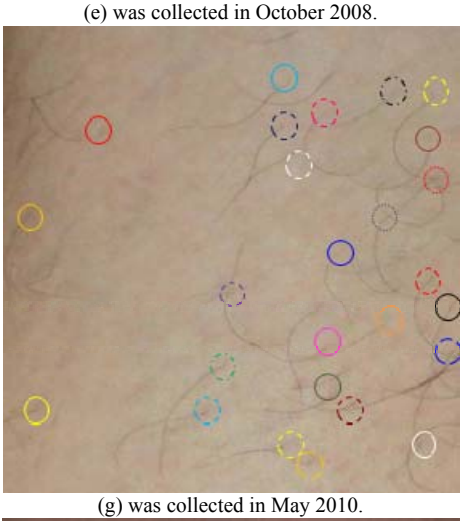

(g) was collected in May 2010.

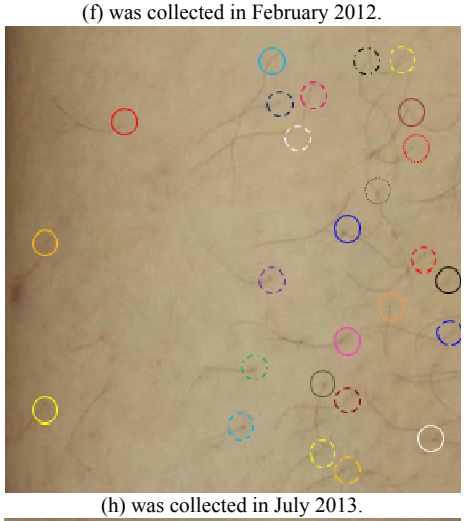

(h) was collected in July 2013.

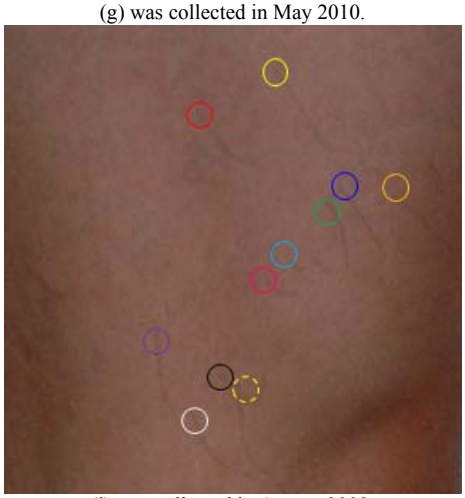

(i) was collected in August 2009.

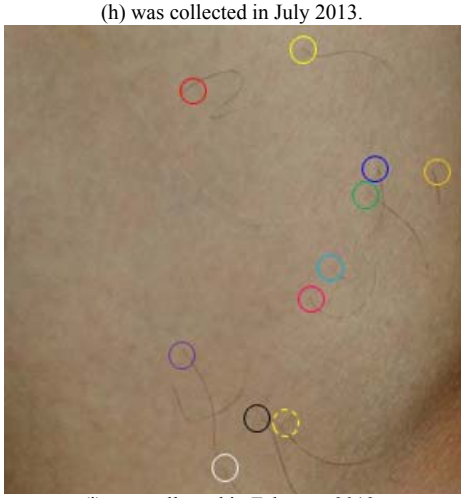

(j) was collected in February 2012.

Fig. 1 Skin images from five legs. Each row shows images from the same leg collected at different time periods. The color circles indicate the partial corresponding androgenic hair follicles.

Forensic scientists have studied hairs for many years. There are two common approaches, microscopic examination and mitochondrial DNA (mtDNA) comparison to analyze hairs collected from crime scenes. The microscopic examination has been accepted as a standard technique for forensic hair comparisons for over 50 years. It has been widely accepted by courts around the world [24, 38-39]. Forensic scientists use microscopes to observe the microscopic features of hairs, including but not limited to cortex cell pigment, cuticle, scale protrusion and medulla, to perform hair comparisons. They performed extensive comparisons on hairs. Wickenheiser et al. and Gaudette et al. performed respectively 366,630 and 431,985 scalp hair comparisons and found that only less than 10 pairs were indistinguishable [25-26]. Forensic scientists studied not only scalp hairs but also pubic hairs [27]. mtDNA is an alternative, which is also accepted by courts [15-16]. In addition to these two standard methods, a nondestructive neutron activation method that measures seventeen chemical

(a) (b) (c) (d)

Fig. 2 Four legs with different androgenic hair patterns.

compounds, an image-based method that extracts statistical features from microscopic images and uses pattern recognition techniques to determine whether or not two hairs come from the same person and a macroscopic feature method that measures hair length, distance and area were also proposed [17-19]. However, they were examined on very small databases. The nondestructive neutron activation, image-based and macroscopic feature methods were respectively examined on hairs from 15, 20 and 8 subjects. These methods, including the microscopic examination and the mtDNA comparison, were developed for hairs collected from crime scenes. They require direct chemical tests and measurements on hairs. It should be emphasized that forensic scientists study hairs collected from crime scenes, while we study patterns formed by androgenic hairs in low resolution images. In addition to forensic analyses, front head hair images were proposed to enhance face recognition systems [20-21] and scalp hair images captured by overhead cameras were proposed for surveillance [22]. Note that scalp hair is in fact not androgenic hair and they have different biological properties. Though the medical research results have implied that androgenic hair can be a reliable biometric trait, we have not found any scientific papers that study androgenic hair patterns in images for criminal and victim identification.

The rest of this paper is organized as follows: Section II presents our database. Section III provides the computational details of the proposed algorithm. Section IV reports the experimental results. Section V discusses the impacts of our findings and lists future research directions of using androgenic hair for criminal and victim identification.

II. An Androgenic Hair Image Database

Different races and body sites have different androgenic hair densities. Indians commonly have dense androgenic hair on their chests and arms, but many eastern Asians such as Chinese do not have. Figs. 3 and 4 show chest and forearm images from Chinese and Indians. Lower legs were chosen for this study because they are the body site most commonly with androgenic hair [23] and often observable in images describing crime-scene specimen (e.g., violent protesters wearing shorts). Though lower legs were selected, androgenic hair in other body sites can also have evidential values.

To study androgenic hair patterns in low resolution images, 1,138 images from 283 legs without tattoos were collected. These images were collected mostly from Asian subjects, including Chinese, Malays and Indians in Singapore using two cameras — a Nikon D70s camera (the maximum resolution of 3,008×2,000 pixels) and a Canon EOS 500D camera (the maximum resolution of 4,752×3,168 pixels). Note that Nikon D70s is a very old model, launched in 2005. Its maximum resolution is only 6 mega pixels, which is even lower than that of current compact cameras. Two image collection occasions

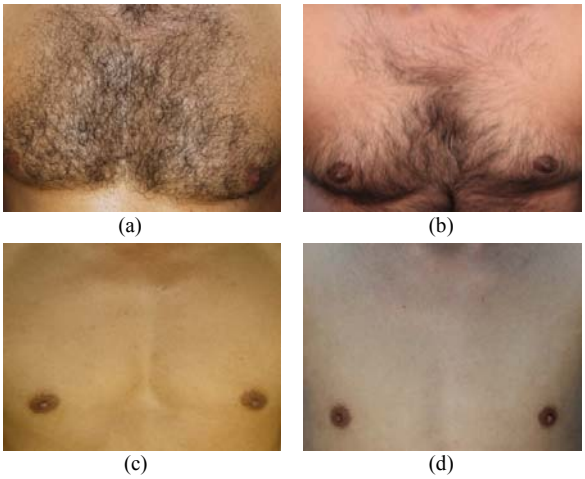

(a) (b) (c) (d)

Fig. 3 Chests with different androgenic hair densities. (a) and (b) are from two Indians and (c) and (d) are from two Chinese.

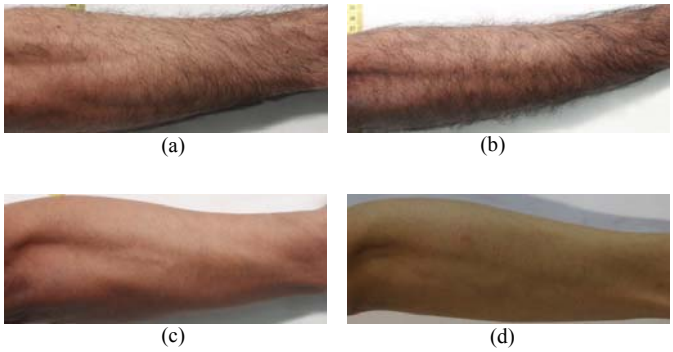

(a) (b) (c) (d)

Fig. 4 Forearms with different androgenic hair densities. (a) and (b) are from two Indians and (c) and (d) are from two Chinese.

with an interval of around 11 days were carried out. In the image collection, we did not give strict instructions to the subjects and allowed illumination changes. Images with diverse quality were thus collected. The quality differences came from different viewpoints, poses, illumination conditions, and image resolutions. The distance between the cameras and the subjects was about 1.6m. In total, images of 11 races, including Arab, Bengali, Caucasian, Chinese, Eurasian, Indian, Indonesian, Javanese, Malay, Punjabi and Vietnamese, were collected. In the first occasion, 575 images from the 283 legs were collected and in the second occasion, 563 images from the same 283 legs were collected. We took one to four images from each subject in each occasion. Table I gives the details. The right lower legs were manually cropped. Figs. 5(a)-(l) show high resolution images of six legs from different viewpoints and illumination conditions. Using the highlighted skin marks, scars and other skin features, these differences can be noted. Their original resolutions were about 4,009 pixels per square centimeter. Fig. 5(m) shows images of 24 different legs, whose relative scale differences are retained. These images were collected from different viewpoints and poses because as mentioned before, we did not give strict instructions to the subjects. The preprocessing scheme presented in Section III.A reduced the image sizes to 142×298, 106×223, 71×149 and 35×74 pixels. The average resolutions of the preprocessed images were respectively 25, 18.75, 12.5 and 6.25 dpi (dots per inch). Their corresponding resolutions in terms of pixels per square centimeter were 97, 54, 24, and 6. Using the Canon EOS 500D camera with a focal length of 55mm and a sensor pixel size of 2.2107×10^{-5} mm^2 to capture original images with these resolutions, the distances between subjects and the camera are respectively 11.9m, 15.8m, 23.8m, and 47.5m. These distances are calculated by the equation, $d = 25.4 \times f/(r \times \sqrt{\rho})$, where f is the focal length, r is the resolution in dpi and ρ is the sensor pixel size in mm^2. Note that one inch is equal to 25.4mm. They indicate that images with these resolutions can be easily captured from a long distance. Fig. 6 shows lower leg images with different resolutions. In these resolutions, skin marks and blood vessels are no longer observable. Fig. 7(a) shows a high resolution image and Figs. 7(b) and (c) show respectively its low resolution versions with 25 dpi and 6.25 dpi. A skin mark, which is highlighted by a rectangle, can be clearly observed in the high resolution image, but it is not observable in the low resolution images. In Section III, preprocessed images with 25 dpi are used to illustrate the proposed algorithm. The experimental results from the preprocessed images with different resolutions are reported in Section IV.

TABLE I
DATABASE DETAILS

Number of images	Number of legs (the first occasion, probe set)	Number of legs (the second occasion, gallery set)
1	5	6
2	265	274
3	12	3
4	1	0

III. THE PROPOSED ANDROGENIC HAIR PATTERN IDENTIFICATION ALGORITHM

The proposed androgenic hair pattern identification algorithm has three computational components, preprocessing, feature extraction and matching. The schematic diagram of the proposed algorithm is given in Fig. 8. The algorithm takes a color leg image as an input and compares it with templates in a

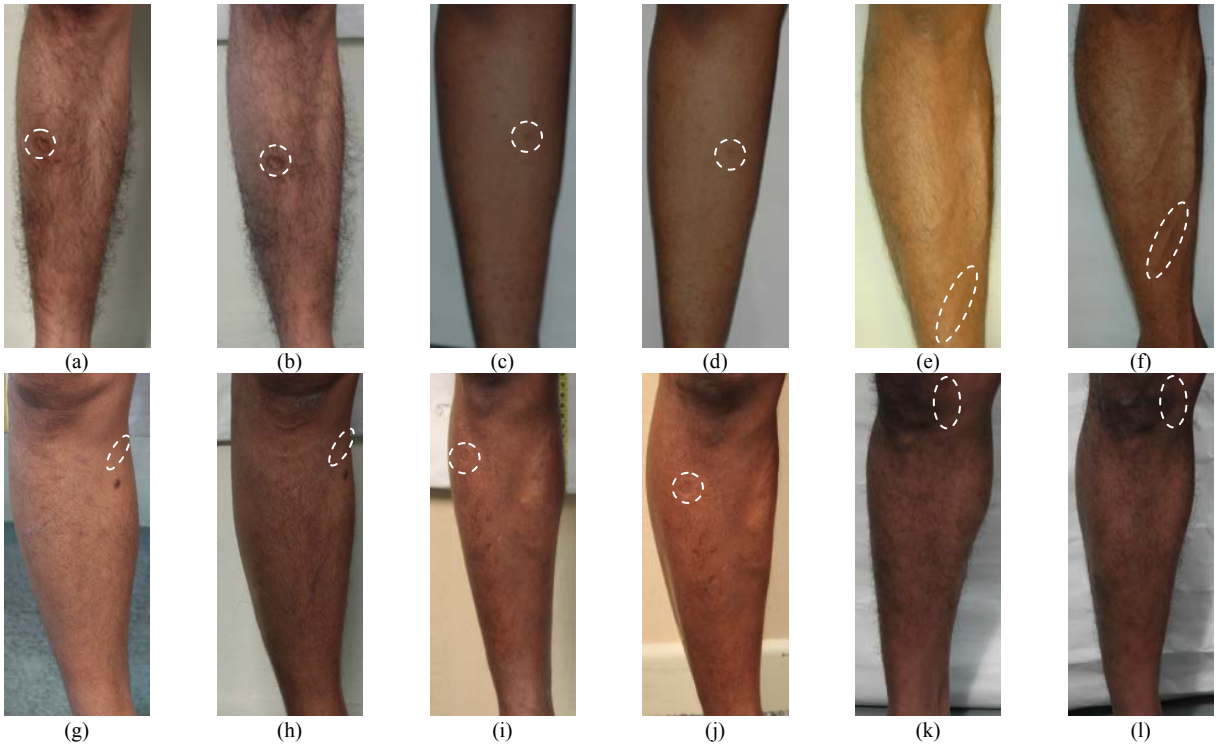

(m)

Fig. 5 Sample images in our database. (a)-(l) image pairs of six legs and (m) images of 24 different legs.

(a) (b) (c) (d)

Fig. 6 (a)-(d) are respectively images with 25, 18.75, 12.5 and 6.25 dpi.

given database. First, the input leg image is segmented and normalized. The segmentation process is to remove all irrelevant information e.g. background. The normalization process is to identify the common region and standardize the image size for matching. Real parts of Gabor filters with different scales and orientations are then applied to the preprocessed image to compute Gabor magnitudes (Fig. 8(c)). These magnitudes are combined to extract local orientations and form an orientation field (Fig. 8(d)). It is divided into small regions for computing local orientation histograms as features (Fig. 8(e)). Each small region is composed of about 300 pixels. Finally, these histograms are matched with those in the database. Section III.A presents the preprocessing scheme and Section III.B presents the feature extraction and matching schemes.

A. Preprocessing

In forensic analysis, images describing crime-scene specimen are always captured in uncontrolled and non-cooperative environments. However, images in a given database can be captured in a controlled environment. These images can be captured from inmates in a prison under strict instructions from prison officers. Images describing crime-scene specimen and images in the database can differ in size, resolution and orientation. These differences should be minimized to increase matching performance. Fig. 9 illustrates the proposed preprocessing scheme. First, input color leg images are segmented. Currently, a semi-automatic approach[#] that is composed of an automatic segmentation scheme and a manual correction process is employed. The automatic scheme uses the skin color and leg boundaries to perform segmentation and is summarized below:

Step 1: An input color image is first converted to a grayscale image for extracting leg boundaries and then is smoothed by a two dimensional median filter. Sobel edge detector is applied to the smoothed grayscale image to obtain an edge image denoted as *J*. The threshold used in this edge detection is automatically determined for every image.

Step 2: A predefined skin color range is used to detect skin pixels in the input color image. If a pixel color is within the color range, it is retained; otherwise, the pixel value is set to zero. More precisely, if the color

[#] The semi-automatic segmentation scheme is used to remove all irrelevant information e.g. background and identify the common region for matching. It is not designed for extracting features.

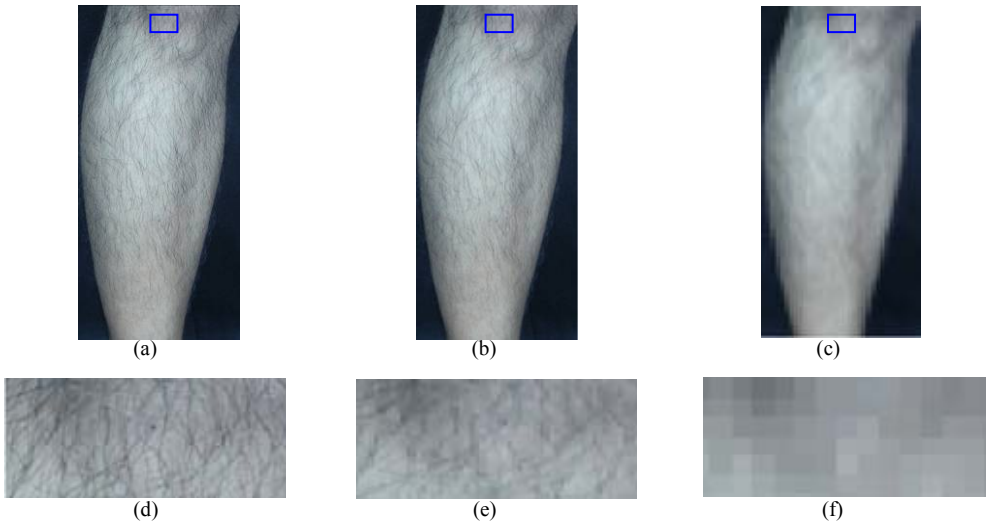

Fig. 7 (a) is a high resolution skin image. (b) and (c) are its low resolution versions with 25 and 6.25 dpi, respectively. (d)-(f) are skin patches with a skin mark from (a)-(c), respectively.

difference between the red channel value and the green channel value of a pixel is less than 5 or greater than 80, this pixel is considered as a non-skin pixel. These parameters were determined by a set of training images. This processed image is denoted as L.

Step 3: In this step, information in J and L is used simultaneously. If a pixel in J is not an edge pixel and the corresponding pixel in L is not zero, the corresponding pixel in the original image is considered as a skin pixel. If the pixel in J is an edge pixel and the corresponding neighborhood in L is not zero, the corresponding pixel in the original image is also considered as a skin pixel. Combining the skin pixels from these two rules, a segmented skin image is obtained.

Step 4: Finally, a morphological operator with a disk-shaped structuring element is applied to the image obtained from Step 3.

After automatically segmenting the image, it was checked manually. If there was a segmentation error, manual segmentation was performed. This semi-automatic approach is acceptable in forensic analysis and is currently used in forensic fingerprint identification. Minutiae in fingermarks are first detected by an automatic algorithm and then corrected and confirmed by fingerprint experts. The segmented color images are converted to grayscale images and the key points defined in Fig. 10 are detected. In Fig. 10, the horizontal distance between B and B' is the shortest one and the horizontal distance between M and M' is the longest one. The horizontal distance between A and A' is the shortest one above the line M and M'. The region of interest is defined based on the most left pixel on the leg boundary between A and B and the most right pixel on the leg boundary between A' and B'. Note that the input images are assumed to be roughly vertical. The region of interest is extracted and resized to 142× 298, 106×223, 71×149 and 35×74 pixels. Resizing the region of interest to these resolutions is to evaluate androgenic hair patterns in low resolution images. Though images are normalized, leg boundaries in different images, even from the same leg, are not completely identical. Fig. 11 shows leg boundaries in two images from the same leg. Some distortions such as illumination variations have not been processed. Our feature extraction and representation schemes presented in the next subsection are designed to tolerate these

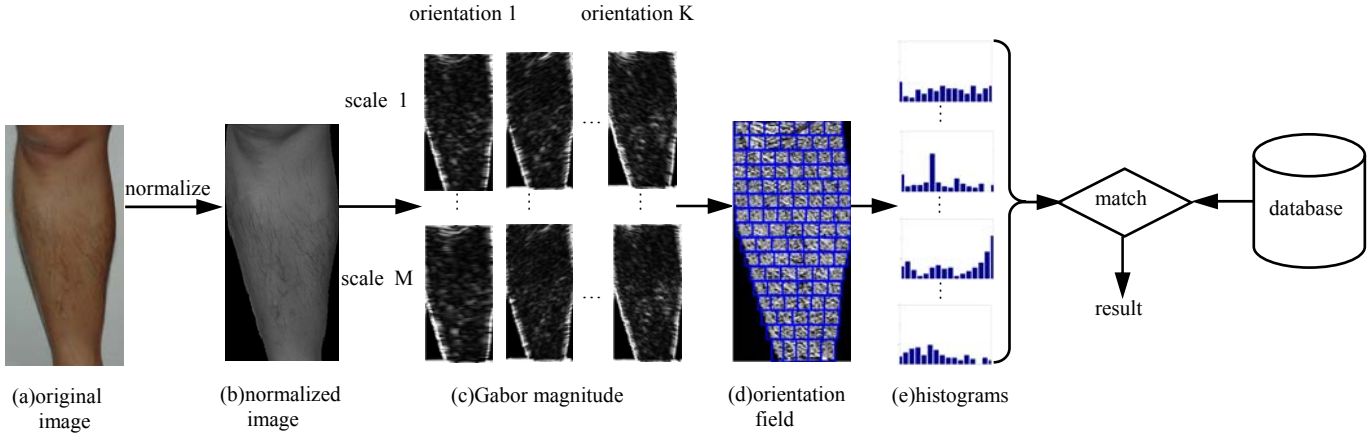

Fig. 8 The schematic diagram of the proposed algorithm.

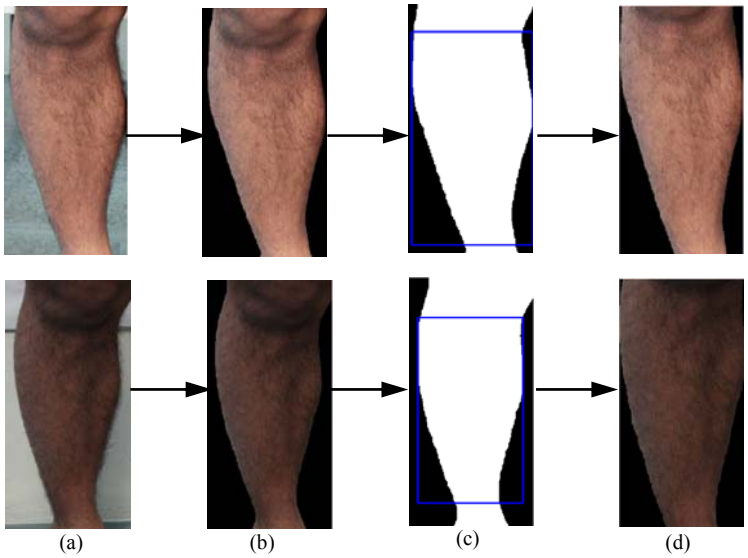

Fig. 9 The proposed preprocessing scheme. (a) input images, (b) segmentation results, (c) regions of interests and (d) preprocessed images. The images in the first and the second rows are from the same leg.

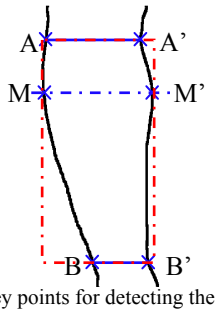

Fig. 10 Key points for detecting the region of interest.

Fig. 11 Leg boundaries in two images from the same leg after preprocessing.

distortions.

B. Gabor Orientation Histograms on a Dynamic Grid System

Local androgenic hair patterns with different orientations and densities contain rich information. We have pinpointed that androgenic hair follicles are very stable, implying that androgenic hair densities are also stable[††]. Androgenic hair orientations are partially determined by their follicle directions. There are different androgenic hair types, including straight, curly and afro-textured. They are genetically dependent. Fig. 12 shows twenty androgenic hair patches from different persons. They are clearly distinctive.

Input images can be collected in uncontrolled environments such as crime scenes, implying that perfect image alignment is difficult to be achieved. This imperfection can be due to non-linear distortion from muscle movement and from the capture conditions (e.g. camera position, angle and focal distance). Point-based feature extraction methods such as IrisCode for iris identification and Competitive Code for palmprint identification are thus not suitable [28-29]. To capture orientation and density information in imperfectly aligned images, Gabor orientation histograms on a dynamic grid system are proposed.

1) Orientation Field Computation

Gabor filters reaching the theoretical limit of uncertainty relation for information offer spatial locality, spatial frequency and orientation selectivity. Numerous scientific studies and commercial systems have demonstrated their feature extraction capability. A study pointed out that Gabor filters can be utilized as a Gabor atom detector and the magnitude and phase of a target Gabor atom can be approximated by the magnitude and phase of the corresponding Gabor response [30]. Gabor filters produce three raw features, phases, magnitudes and orientations. Another study compared these features on face images and concluded that the orientation feature is the most distinctive and robust feature [31]. The orientation feature was also used for palmprint identification [60]. Though face, palmprint and androgenic hair images are different types of images, their orientation information is clear. Androgenic hairs can be regarded as line segments with different orientations and scales. In high resolution images, if locations of follicles and directions of androgenic hairs can be extracted, androgenic hair features are similar to minutia features. To capture orientation information and handle scale variation, the proposed algorithm uses real parts of Gabor filters, which are defined as

Fig. 12 Androgenic hair patches.

[††] The term stable refers to the stability of biological properties of androgenic hair patterns. Note that hair patterns can be altered through hair removal cream and shavers easily.

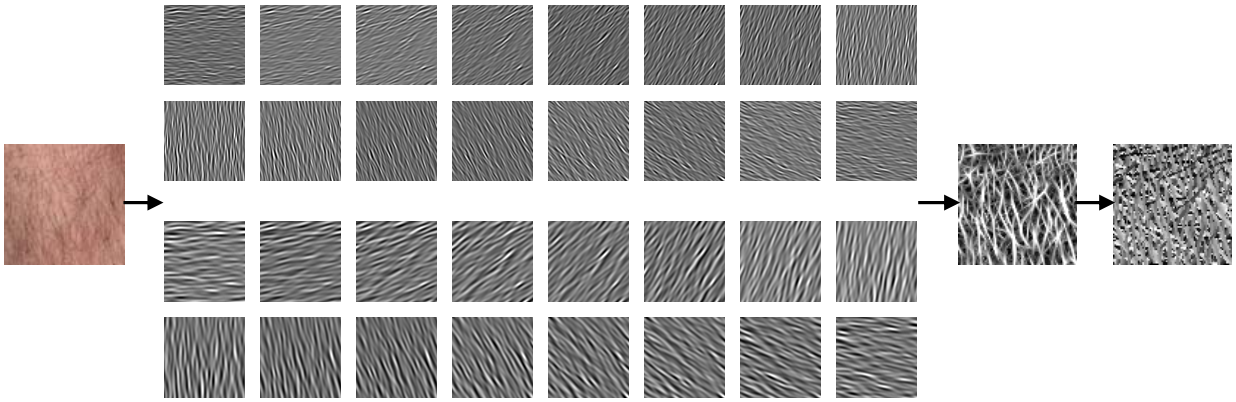

(a) (b) (c) (d)

Fig. 13 The computational process of orientation fields. (a) an image patch, (b) the filter responses from a Gabor filter bank with 16 orientations and 2 scales, (c) the magnitude field and (d) the orientation field.

$$G(x,y,\lambda_{mk},\theta_k,\sigma_m,\gamma)=\frac{\gamma}{2\pi\sigma_m^2}\exp\left(-\frac{x'^2+\gamma y'^2}{2\sigma_m^2}\right)\cos\left(\frac{2\pi x'}{\sigma_{mk}}\right), \quad (1)$$

where $x'=x\cos\theta_k+y\sin\theta_k$ and $y'=-x\sin\theta_k+y\cos\theta_k$ are the rotated coordinates with orientation $\theta_k=k\pi/8$, λ_{mk} denotes the wavelength of the sinusoidal component, σ_m is the standard deviation of the elliptical Gaussian window along x' direction, γ is the spatial aspect ratio, $m\in\{1,\cdots,M\}$ and $k\in\{1,\cdots,K\}$ are the scale and orientation indexes respectively. To enhance robustness against brightness variation, the direct current (DC) component in Eq. 1 is removed. In total, $M\times K$ real parts of Gabor filters with zero DC are applied to the preprocessed images.

Let $I(x,y)$ be a preprocessed image and $G_{rd}(x,y,\lambda_{mk},\theta_k,\sigma_m,\gamma)$ be a real part of a Gabor filter with zero DC. The filter response $F_{\lambda_{mk},\theta_k,\sigma_m,\gamma}(x,y)$ can be obtained from

$$F_{\lambda_{mk},\theta_k,\sigma_m,\gamma}(x,y)=G_{rd}(x,y,\lambda_{mk},\theta_k,\sigma_m,\gamma)*I(x,y), \quad (2)$$

where $*$ denotes an operation of a two-dimensional convolution. The orientation of a pixel is calculated by

$$O(x,y)=\arg_{\theta_k}\max_{m,k}M_{\lambda_{mk},\theta_k,\sigma_m,\gamma}(x,y), \quad (3)$$

where $M_{\lambda_{mk},\theta_k,\sigma_m,\gamma}(x,y)$ denotes the magnitude of $F_{\lambda_{mk},\theta_k,\sigma_m,\gamma}(x,y)$. Since $F_{\lambda_{mk},\theta_k,\sigma_m,\gamma}(x,y)$ is real, $M_{\lambda_{mk},\theta_k,\sigma_m,\gamma}(x,y)$ can be computed from

$$M_{\lambda_{mk},\theta_k,\sigma_m,\gamma}(x,y)=\left|F_{\lambda_{mk},\theta_k,\sigma_m,\gamma}(x,y)\right|. \quad (4)$$

$O(x,y)$ is called the orientation field and $\max_{m,k}M_{\lambda_{mk},\theta_k,\sigma_m,\gamma}(x,y)$ is called the magnitude field. Fig. 13 shows an image patch, filter responses and the corresponding magnitude and orientation fields. The orientation field clearly captures the androgenic hair orientations. Fig. 14 shows the orientation difference between a pure skin region and a hair region. Fig. 14(a) is a skin patch with androgenic hairs and pure skin regions. Figs. 14(b) and (c) are local magnitude fields generated from $\max_{m,k}M_{\lambda_{mk},\theta_k,\sigma_m,\gamma}(x,y)$. They are computed from 32 zero DC Gabor filters with 16 orientations and 2 scales i.e., $k\in\{1,\cdots,16\}$ and $m\in\{1,2\}$. Their orientation fields are given in Figs. 14(d) and (e), where the numbers are the orientation index k. Figs. 14(c) and (e) indicate that the androgenic hair patch in Fig. 14(a) produces strong filter response and consistent orientations. However, the pure skin patch in Fig. 14(a) does not provide clear orientation information in Figs. 14(b) and (d). This figure demonstrates that the orientation field can effectively capture orientation information from androgenic hairs.

2) Orientation Field Histograms and Matching

Orientations, positions and densities of androgenic hair patterns are important features. Global descriptors are not desirable because they completely neglect position information. Even in the same leg, image patches in different regions can be very different (Fig. 15). As mentioned before, perfect alignment is not expected and even the boundaries in two preprocessed images from the same leg are not completely identical (Fig. 11). To address these problems, orientation histograms on a dynamic grid system are used as descriptors. Though Gabor filters have been widely applied, we do not note that these descriptors were used before.

To compute orientation histograms, the preprocessed images are derived into rectangular blocks to alleviate problems from imperfect alignment and retain spatial relationships among different androgenic hair regions. Fig. 16 shows the rectangular blocks on three preprocessed images. Note that the blocks are not overlapping and have different sizes (Fig. 16). There are around 300 pixels in each block. A preprocessed image is divided into E rows. Each row is further divided into many blocks. Fig. 16(a) illustrates the rows and the blocks, where E is sixteen. In each row, the number of blocks is not the same. The number of blocks in the i^{th} row is determined by

$$N_i=\left\lfloor\frac{E}{2}\times\frac{\mu_{is}}{\mu_{ia}}+0.5\right\rfloor, \quad (5)$$

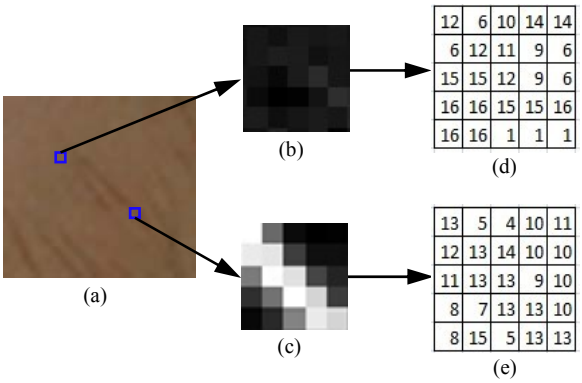

Fig. 14 An example of the local orientations. (a) an original skin image, (b) and (c) are local magnitude fields from the two image patches and (d) and (e) are respectively their orientation fields in integer representation.

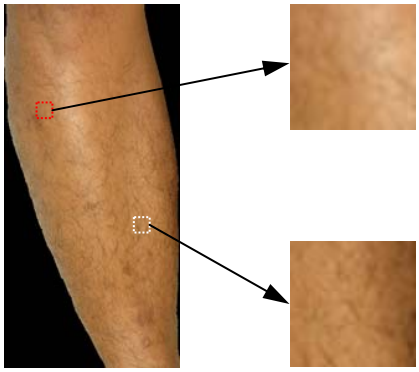

Fig. 15 Image patches from the same image.

where $i = 1, \cdots, E$, μ_{is} is the average number of skin pixels in the i^{th} row, μ_{ia} is the total number of pixels, including background pixels in the i^{th} row and $\lfloor\ \rfloor$ denotes a floor operator. The red rectangle in Fig. 16(a) illustrates μ_{ia}. In total, a preprocessed image is divided into $N = \sum_{i=1}^{E} N_i$ blocks. Note that the number of blocks in each image is the same, but their sizes can be different (Fig. 16). This dynamic grid system is designed to deal with distortions that are not well handled by the preprocessing scheme.

In each block, one histogram is computed from the orientation field. In total, N histograms are obtained. Since the block sizes in different images are not the same, the histograms have to be normalized. The bin values in the normalized histograms are in the range between zero and one and the summation of all bin values is one. A normalized histogram is in fact a distribution. Mathematically, a normalized histogram of a block is computed by

$$h_{OB_j}(k) = \frac{1}{|B_j|} \sum_{(x,y)\in B_j} \delta(O(x,y) = k), \qquad (6)$$

where B_j is a set containing coordinates of the pixels in the j^{th} block, $|B_j|$ is the cardinality of B_j, δ is the Kronecker delta function and k is an orientation index. These histograms are called Gabor orientation histograms. The first row in Fig. 17 gives six local androgenic hair patterns and the second row gives the corresponding Gabor orientation histograms. It demonstrates that Gabor orientation histograms can describe skin without androgenic hairs and skin with various androgenic hair patterns. Figs. 17(c) and (d) are two skin patches from the same location of the same leg but different images. Figs. 17(i) and (j) indicate that their histogram similarity is very high. Figs. 17(e) and (f) are another two skin patches from the same location of the same leg but different images. We can also observe the same characteristics in Figs. 17(k) and (l).

Given two sets of Gabor orientation histograms, $H_{O_i} = \{h_{O_iB_1}, \cdots, h_{O_iB_N}\}$ and $H_{O_d} = \{h_{O_dB_1}, \cdots, h_{O_dB_N}\}$, from respectively an input image and a registered image in a database, the blockwise Chi-square distance defined as

$$X(H_{O_i}, H_{O_d}) = \sum_{t=1}^{N}\sum_{k=1}^{K} \frac{(h_{O_iB_t}(k) - h_{O_dB_t}(k))^2}{h_{O_iB_t}(k) + h_{O_dB_t}(k)}, \qquad (7)$$

is used to measure their dissimilarity.

IV. Experimental Results

In the experiments, the images collected in the first occasion were considered as a probe set and the images collected in the second occasion were considered as a gallery set. Cumulative match curves (CMC) and rank-one accuracies were used as performance indicators. Note that the database information has been given in Section II. Most of the legs in the database have

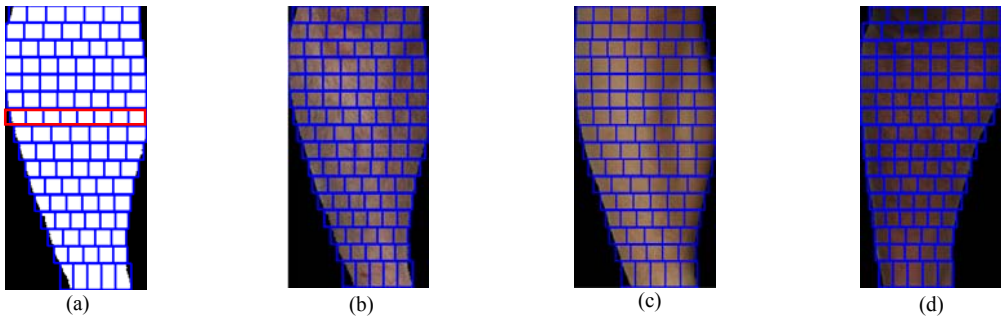

Fig. 16 Illustration of the dynamic grid system. (a) the dynamic grid system and (b)-(d) leg images overlaid with the blocks generated from the dynamic grid system.

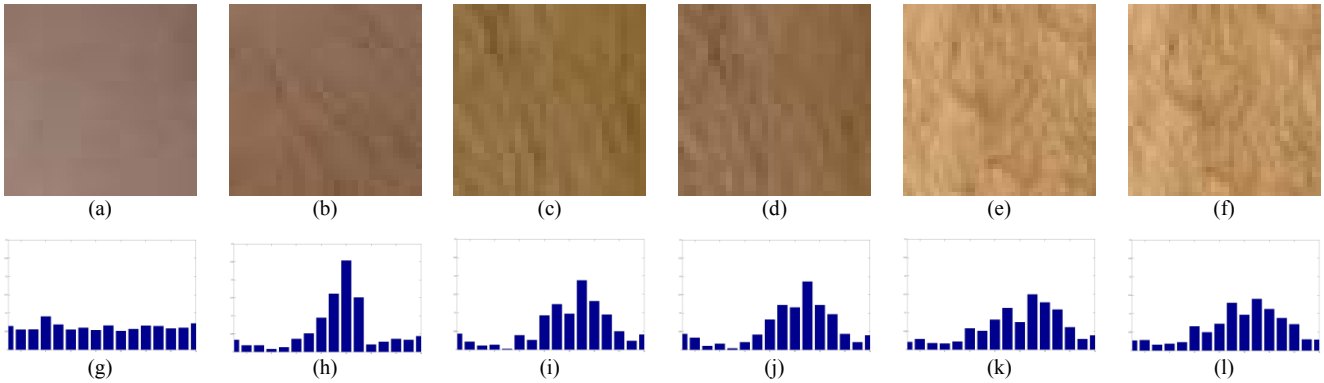

Fig. 17 Androgenic hair patterns and their orientation histograms. The first row is image patches from four legs and the second row is the corresponding Gabor orientation histograms. (c) and (d) are two image patches from the same location of the same leg but different images. (e) and (f) are another two image patches from the same location of the same leg but different images.

two images in the gallery and probe sets.

The first experiment aimed to determine the parameter E, which controls the number of blocks. 128 Gabor filters with 32 orientations and 4 scales were used. The size of the preprocessed images was 142×298 pixels. The rank-one accuracies for E=8, E=16 and E=32 were 76.17%, 77.91% and 57.74% respectively. The second experiment aimed to determine the parameter K in the Gabor filter bank, which controls the number of orientations. In this experiment, E was set to sixteen and the corresponding total number of blocks was 108. The rank-one accuracies for K =8, K =16, K =32 and K =64 were 75.83%, 76.87%, 77.91% and 76.17% respectively. In the rest of the experiments, E was set to 16 and K was set to 32.

We compared the proposed algorithm with the local binary pattern (LBP) methods [32-34], including $LBP_{8,1}^{riu2}$, $LBP_{8,1}^{ri}$, $LBP_{8,1}^{u2}$, $LBP_{8,2}^{riu2}$, $LBP_{8,2}^{ri}$, $LBP_{8,2}^{u2}$, $LBP_{16,2}^{riu2}$ and $LBP_{16,2}^{u2}$, the local Gabor binary pattern (LGBP) methods [35], including $LGBP_{8,1}^{riu2}$, $LGBP_{8,1}^{u2}$, $LGBP_{8,2}^{riu2}$ and $LGBP_{8,2}^{u2}$ and the histograms of oriented gradients (HOG) method [36] on grayscale images and red, green and blue channel images. In these comparisons, the size of the preprocessed images was 142×298 pixels. Table 2 lists the feature dimensions of these methods. Fig. 18 shows the CMCs of the best LBP, LGBP and HOG methods and the proposed algorithm from the corresponding optimal channels. $LBP_{8,1}^{u2}$ on the green channel is the best LBP method and $LGBP_{8,1}^{u2}$ on the green channel is the best LGBP method. HOG performs the best on the grayscale images. In this comparison, the proposed algorithm is the best. The rank-one accuracy of the proposed algorithm on the grayscale images is 1.91% higher than that of $LBP_{8,1}^{u2}$ on the green channel images. It is also 1.91% higher than that of $LGBP_{8,1}^{u2}$ on the green channel images and 19.82% higher than that of the HOG method on the grayscale images. The numbers of images which were correctly identified by the proposed algorithm, but incorrectly identified by $LBP_{8,1}^{u2}$, $LGBP_{8,1}^{u2}$ and HOG on the corresponding optimal channels are 58, 53 and 133, respectively. 31 of them were incorrectly identified by $LBP_{8,1}^{u2}$, $LGBP_{8,1}^{u2}$ and HOG. Fig. 19 shows some of these images. The feature dimensions of the proposed algorithm, $LBP_{8,1}^{u2}$, $LGBP_{8,1}^{u2}$ and the HOG method are 3456, 6372, 254880 and 8748, respectively. Most of the legs in our database have androgenic hair and therefore, the discriminative power is from androgenic hair patterns, instead of skin texture.

TABLE II
FEATURE DIMENSIONS OF DIFFERENT METHODS

Methods	Feature dimensions
$LBP_{8,1}^{riu2}$, $LBP_{8,2}^{riu2}$	1080 (10*108)
$LBP_{8,1}^{ri}$, $LBP_{8,2}^{ri}$	3888 (36*108)
$LBP_{8,1}^{u2}$ $LBP_{8,2}^{u2}$	6372 (59*108)
$LBP_{16,2}^{riu2}$	1944 (18*108)
$LBP_{16,2}^{u2}$	26244 (243*108)
$LGBP_{8,1}^{riu2}$, $LGBP_{8,2}^{riu2}$	43200 (10*40*108)
$LGBP_{8,1}^{u2}$, $LGBP_{8,2}^{u2}$	254880 (59*40*108)
HOG	8748 (81*108)
The proposed algorithm	3456 (32*108)

This experiment aimed to evaluate the proposed algorithm on androgenic hair patterns in very low resolution images. The preprocessed images were first resized to 142×298, 106×223, 71×149 and 35×74 pixels and the corresponding resolutions were respectively 25, 18.75, 12.5 and 6.25 dpi. Then, we scaled these images up back to 142 × 298 pixels so we did not need to change the parameters in the proposed algorithm. Fig. 20 shows that when the image sizes decrease, the accuracies also decrease. The images with resolutions of 25 and 18.75 dpi provide a similar performance. The performance drops relatively significant for the images with resolutions of 12.5 and 6.25 dpi. Their rank-one accuracies are still over 71% and 64%, respectively. These experimental results demonstrate that androgenic hair patterns even in low resolution images are an effective biometric trait.

This experiment aimed to evaluate the proposed algorithm on androgenic hair patterns from the same race. 52.7%, 32.2% and 7.4% of the subjects in our database are Chinese, Malays and Indians, respectively. Fig. 21 shows different androgenic hair patterns from the same race and Fig. 22 shows the identification results. More clearly, the gallery and probe sets were all from the same race and the resolution of the images was 25 dpi. These figures show that androgenic hair patterns from the same race are different enough for identification.

The last experiment aimed to evaluate androgenic hair patterns and the proposed algorithm for identification with a large gallery set. The number of images in the probe set was still 575 images from the 283 right legs, but the number of images in the gallery set was increased to 1,111 images from 558 legs of the 283 subjects. Since the left legs of eight subjects have tattoos, they were excluded from this experiment. The left leg images were flipped and therefore, they could be regarded as right legs. The resolution of the images was 25 dpi. To avoid genetic factors influencing the results, the images from the left and right legs of the same person were not allowed to match. Fig. 23 shows the CMCs. Even though the gallery set was increased to 1,111 images, the rank one identification accuracy is still over 72%. It shows the effectiveness of androgenic hair patterns for identification with a large gallery set.

V. Discussion and Future Work

Identifying criminals and victims in images describing crime-scene specimen is a challenging task, especially when neither faces nor tattoos are observable. Though blood vessel patterns and skin mark patterns have been proposed to address this problem, they demand high resolution images to visualize hidden blood vessels and accurately detect skin marks. This paper first provides a list of medical studies and images to justify that androgenic hair patterns are a stable biometric trait. Though hairs collected in crime scenes are regularly used for forensic analysis, according to our best knowledge, androgenic hair patterns in images were never studied for criminal and victim identification. For matching androgenic hair patterns, we propose an algorithm based on a dynamic grid system and Gabor orientation histograms. The experimental results on a database containing 4,552 images from 283 different legs with resolutions of 25, 18.75, 12.5 and 6.25 dpi demonstrate two points: androgenic hair patterns in low resolution images are an effective biometric trait and the proposed Gabor orientation histograms are comparable with other well-known texture recognition methods, including local binary patterns, local Gabor binary patterns and histograms of oriented gradients. This paper exposes a new way to address the challenging criminal and victim identification problem.

In forensic identification, image quality is always a problem. Images of child pornography, masked gunmen and violent protestors are our targets. Child pornographic images often have good quality because pedophiles enjoy high quality images. For cases of masked gunmen and violent protectors, the original images can be taken by reporters, who always use professional DSLR cameras, e.g. Canon EOS 10DX. Sometimes good quality images are obtained. For web images describing crime-scene specimen, no matter what cameras are used to take the original images, one great challenge is low resolution, which is the focus of this paper. Although the resolution of surveillance videos is also very low, the challenges in surveillance images and web images are different. Surveillance cameras are always mounted in high positions. They likely capture head-print, instead of androgenic hair [22].

This paper demonstrates that androgenic hair patterns in low resolution images can be used as a biometric trait for criminal and victim identification. However, low resolution is only one of the problems. For robust identification, new algorithms should be developed for viewpoint and pose variations and occlusions. These algorithms can enhance the performance of the proposed algorithm, which uses the dynamic grid system and the features to absorb all variations and distortions. In addition, an automatic segmentation algorithm should be developed to reduce manpower, even though a semi-automatic approach is not uncommon in forensic analysis. Our database size is comparable with other biometric databases for scientific

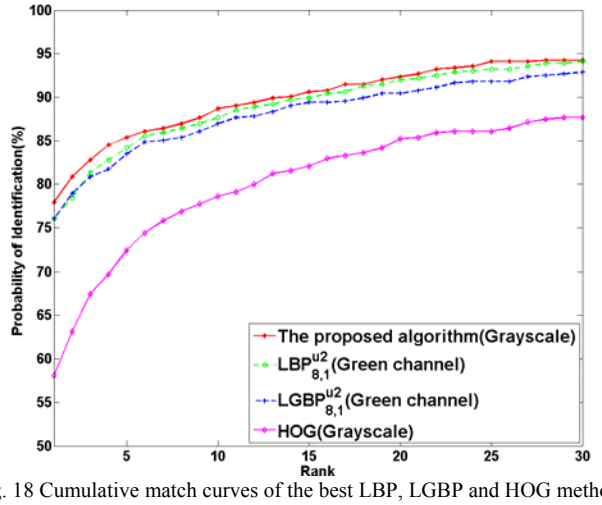

Fig. 18 Cumulative match curves of the best LBP, LGBP and HOG methods and the proposed algorithm from the corresponding optimal channels.

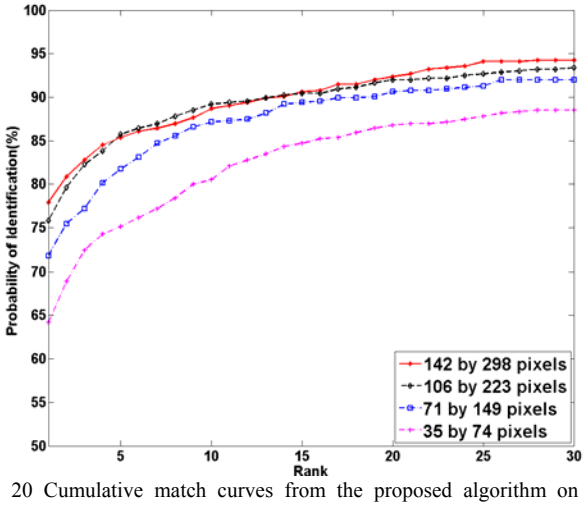

Fig. 20 Cumulative match curves from the proposed algorithm on low resolution images.

Fig. 19 Five sets of images which were correctly identified by the proposed algorithm, but incorrectly identified by $LBP^{u2}_{8,1}$, $LGBP^{u2}_{8,1}$ and HOG on the corresponding optimal channels. The first column is the images in the probe set. The 2nd-5th columns are the corresponding rank one images given by the proposed algorithm, $LBP^{u2}_{8,1}$, $LGBP^{u2}_{8,1}$ and HOG on the optimal channels, respectively.

studies e.g. West Virginia University iris database, but it is small comparing with fingerprint databases in law enforcement agents. We will continue collecting more images for algorithm development and evaluation. Once law enforcement agents use androgenic hair patterns in real applications, numerous images can be collected from inmates and suspects for this research direction. Though low resolution images are the focus of this paper, androgenic hairs and their follicles in high resolution images should also be studied, because in child pornography cases, high resolution and close up images are commonly obtained. In addition to searching a suspect in a given database, how to assign evidential values in the form of a likelihood ratio

to androgenic hair patterns is also equally important [61]. More detailed description of forensic biometric applications can be found in [65]. In this paper, a list of medical studies and images are given to justify that androgenic hair is a stable biometric trait. A large-scale study for determining the permanence of androgenic hair is still demanded. Since each hair has its own rhythm and hair shafts fall out at different time, how these issues impact matching accuracy should also be further studied.

In addition to androgenic hair, our research group is studying blood vessel patterns hidden in color images and Relatively Permanent Pigmented or Vascular Skin Marks (RPPVSM) for criminal and victim identification [13-14, 61]. These features

Fig. 21 Different androgenic hair patterns from the same race. The first, second and third rows are androgenic hair patterns from Chinese, Malays and Indians, respectively.

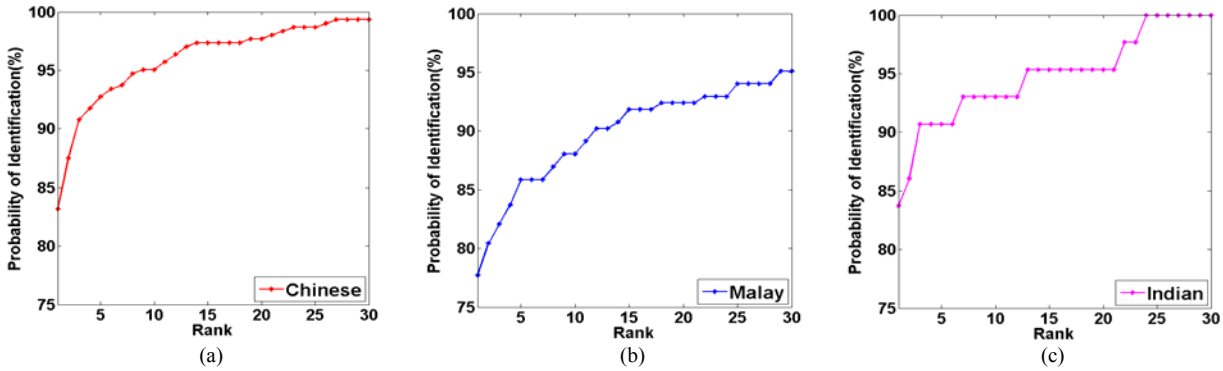

(a) (b) (c)

Fig. 22 Cumulative match curves from the same race. (a) Chinese, (b) Malays and (c) Indians.

and androgenic hair should be used simultaneously when they are available. We aim finally to develop a powerful system to identify criminals and victims and link different cases based on non-facial skin in images describing crime-scene specimens.

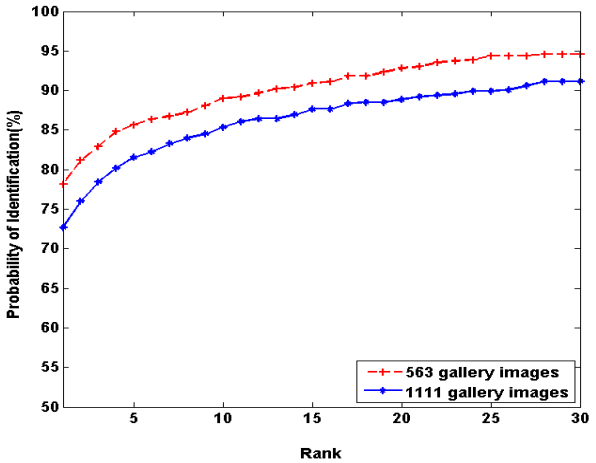

Fig. 23 The cumulative match curves from the gallery sets with 563 images and 1,111 images.

ACKNOWLEDGMENTS

We would like to thank the U.S. Department of Justice, the Immigration and the Customs Enforcement, the Singapore Prison Service and the Singapore Police Force for their legal and forensic discussions and Frodo Chan for preparing the images in the last experiment. This work is partially supported by the Ministry of Education, Singapore through Academic Research Fund Tier 2, MOE2012-T2-1-024.

REFERENCES

[1] M. Motivans and T. Kyckelhahn, "Federal prosecution of child sex exploitation offenders, 2006", *Bureau of Justice Statistics Bulletin*, pp. 1-8, 2007.
[2] BBC News, "International child porn ring smashed", 26 March 2001. Available: http://news.bbc.co.uk/1/hi/world/americas/1244457.stm
[3] Canada's National Tipline for Reporting the Online Sexual Exploitation of Children. Available: http://www.cybertip.ca/pdfs/fact_sheet_pdfs/English/CyberStats_en.pdf
[4] Translation of Sahih Bukhari, vol. 7, book 72, number 815.
[5] H. Zhang, C. Tang, A.W.K. Kong and N. Craft, "Matching vein patterns from color images for forensic investigation", *BTAS*, 2012, pp. 77-84.
[6] J.-E. Lee, R. Jin, A.K. Jain and W. Tong, "Image retrieval in forensics: tattoo image database application", *IEEE Multimedia*, vol. 19, no. 1, pp. 40-49, 2012.
[7] K.S. Stenn and R. Paus, "Controls of hair follicle cycling", *Physiological Reviews*, vol. 81, no. 1, pp. 449-491, 2001.
[8] R.E. Billingham, "A reconsideration of phenomenon of hair neogenesis with particular reference to the healing of cutaneous wounds in adult mammals". In: W. Montagna and RA Ellis (eds) The biology of hair growth. Academic Press, New York, 1958.
[9] A. Vogt, K.J. McElwee and U. Blume-Peytavi, "Biology of the hair follicle", in U. Blume-Peytavi, A. Tosti, D.A. Whiting and R.M. Trüeb (Eds) Hair Growth and Disorders, Springer, 2008.
[10] H.B. Chase, "Growth of hair", *Physical Review*, vol. 34, pp. 113-126, 1954.
[11] J.B. Hamilton, "Age, sex and genetic factors in the regulation of hair growth in man: a comparison of Caucasian and Japanese populations", in Montagna W. Ellis RA (eds) The biology of hair growth. Academic Press, New York, pp. 399-433, 1958.
[12] J.B. Hamilton, "Effect of castratio in adolescent and young adult males upon further changes in the proportions of bare and hairy scalp", *Journal of Clinical Endorcrinology & Metabolism*, vol. 20, pp. 1309-1318, 1960.
[13] A. Nurhudatiana, A.W.K. Kong, K. Matinpour, S.Y. Cho and Noah Craft, "Fundamental statistics of relatively permanent pigmented or vascular skin marks", *Proc. of International Joint Conference on Biometrics*, 2011, pp. 1-6.
[14] C. Tang, A.W.K. Kong and Noah Craft, "Uncovering vein patterns from color skin images for forensic analysis", *CVPR*, 2011, pp. 665-672.
[15] C.A. Linch, S.L. Smith and J.A. Prahlow, "Evaluation of the human hair root for DNA typing subsequent to microscopic comparison", *Journal of Forensic Science,* vol. 43, pp. 305-314, 1998.
[16] M. Allen, A.S. Engström, S. Meyers, O. Handt, T. Saldeen, A. von Haeseler, S. Pääbo and U. Gyllensten, "Mitochondrial DNA sequencing of shed hairs and saliva on robbery caps: sensitivity and matching probabilities", *Journal of Forensic Science*, vol. 43, pp. 535-464, 1998.
[17] S.Y. Cho, S.G. Jang and Y.S. Chung, "Human hair identification by instrumental neutron activation analysis", *Journal of Radioanalytical and Nuclear Chemistry*, vol. 229, no. 1-2, pp. 143-147, 1998.
[18] M.S. Verma, L. Pratt, C. Ganesh and C. Medina, "Hair-MAP: a prototype automated system for forensic hair comparison and analysis", *Forensic Science International*, vol. 129, pp. 168-186, 2002.
[19] H. Sato, "Preliminary study of hair form of Japanese head hairs using image analysis", *Forensic Science International*, vol. 131, no. 202-208, 2003.
[20] Y. Yacoob and L.S. Davis, "Detection and analysis of hair", *TPAMI*, vol. 28, no. 7, pp. 1164-1169, 2006.
[21] A. Dantcheva and J.L. Dugelay, "Frontal-to-side face re-identification based on hair, skin and clothes patches", *Proc. IEEE International Conference on Advanced Video and Signal-Based Surveillance*, 2001, pp. 309-313.
[22] H. Aradhye, M. Fishler, R. Bolles and G. Myers, "Headprint — person reacquisition using visual features of hair in overhead surveillance video", *Proc. Audio- Video-Based Biometric Person Authentication*, 2005, pp. 879-890.
[23] S.M. Garn, "Types and distribution of the hair in man", *Annals of the New York Academy of Sciences*, vol. 53, pp. 498-507, 1951.
[24] M.M. Houck, R.E. Bisbing, T.G. Watkins and R.P. Harmonm, "Locard exchange: the science of forensic hair comparisons and the admissibility of hair comparison evidence: Frye and Daubert Considered", *Modern Microscopy Journal*, March, 2004.
[25] B.D. Gaudettee and E.D. Keeping, "An attempt at determining probabilities in human scalp hair comparison", *Journal of Forensic Sciences*, vol. 19, pp. 599-606, 1974.
[26] R.A. Wickenhesier and D.G. Hepworth, "Further evaluation of probabilities in human scalp hair comparison", *Journal of Forensic Sciences*, vol. 35, pp. 1323-1329, 1990.
[27] B.D. Gaudettee, "Probabilities and human public hair comparisons", *Journal of Forensic Sciences*, vol. 31, pp. 514-517, 1976.
[28] J.G. Daugman, "High confidence visual recognition of persons by a test of statistical independence", *TPAMI*, vol. 15, no. 11, pp. 1148-1161, 1993.
[29] A.W.K. Kong, D. Zhang and M. Kamel, "An analysis of brute-force break-ins of a palmprint authentication system", *TSMC, Part B*, vol. 36, no. 5, pp. 1201-1205, 2006.
[30] A. Kong, "An analysis of Gabor detection", *Proc. of International Conference on Image Analysis and Recognition*, 2009, pp. 64-72.
[31] A. Kong, "An evaluation of Gabor orientation as a feature for face recognition", *ICPR*, 2008, pp. 1-4.
[32] T. Ojala, M. Pietikäinen, and T. Mäenpää, "Gray scale and rotation invariant texture classification with local binary patterns", *ECCV*, 2000, pp. 404-420.
[33] T. Ahonen, A. Hadid and M. Pietikainen, "Face description with local binary patterns: application to face recognition", *TPAMI*, vol. 28, no.12, pp. 2037 - 2041, 2006.
[34] D. Huang, C. Shan, M. Ardabilian, Y. Wang and L. Chen, "Local binary patterns and its application to facial image analysis: a survey", *TSMC, Part C: Applications and Reviews*, vol. 41, no. 6, pp. 765 - 781, 2011.
[35] W. Zhang, S. Shan, W. Gao, X. Chen and H. Zhang, "Local Gabor binary pattern histogram sequence (LGBPHS): a novel non-statistical model for face representation and recognition", *ICCV*, 2005, pp. 786 - 791.
[36] N. Dalal and B. Triggs, "Histograms of oriented gradients for human detection", *CVPR*, 2005, pp. 886 - 893.
[37] The National Science and Technology Council's Subcommittee on Biometrics, "Biometrics Glossary", pp. 1-33, 2006.
[38] J. Robertson, Forensic examination of hair, Taylor & Francis (ed), London, 1999.

[39] C.T. Oien, "Forensic hair comparison: background information for interpretation", *Forensic Science Communications*, vol. 11, no. 2, 2009. Online available: http://www.fbi.gov/about-us/lab/forensic-science-communications/fsc/april2009/review/2009_04_review02.htm/.
[40] Images from Bahrain riot: http://imgur.com/r/HumanPorn/LshlQYw.
[41] Images from Bahrain riot: http://www.salon.com/2012/09/18/the_middle_ easts_secret_revolution/.
[42] Images from Turkey riot: http://www.al-monitor.com/pulse/originals/2013/06/erdogan-blames-foreign-hand-in-turkey-protests.html.
[43] Images from Turkey riot: http://www.guardian.co.uk/world/2013/may/31/istanbul-protesters-violent-clashes-police.
[44] Images from London riots: http://www.theage.com.au/world/london-riots-spread-as-police-lose-control-20110809-1ijmm.html.
[45] Images from Athens riots: http://www.ethnos.gr/article.asp?catid=22768&subid=2&pubid=63179258.
[46] Images from Athens riots: http://www.dailyrecord.co.uk/news/uk-world-news/greece-tear-gas-and-stun-grenades-1105563.
[47] Images from Athens riots: http://www.dailymail.co.uk/news/article-2009437/Greek-vote-Rioters-stone-MP-Greece-pushes-austerity-package.html.
[48] Images from Greece riots: http://www.dailymail.co.uk/news/article-2125686/Riots-erupt-Greece-martyr-Dimitris-Christoulas-shoots-debt-crisis.html.
[49] Images from Pakistan riots: http://news.pkvids.com/2012/09/21/pakistan-protests-against-anti-muslim-film-turn-violent/.
[50] Terrorist images: http://nationalmirroronline.net/new/expatriate-workers-terrorist-group-claims-responsibility-for-abduction/.
[51] Terrorist images: http://www.breitbart.com/Big-Peace/2013/02/20/Boko-Haram-Kidnaps-French-Family-in-Cameroon.
[52] Terrorist images: http://tammybruce.com/2010/08/hamas-agrees-with-obama-and-support-gz-mosque.html.
[53] Terrorist images: http://naijamayor.com/new-islamic-terror-group-emerges-in-nigeria-called-movement-for-oneness-and-jihad-in-west-africa-mojao/.
[54] Terrorist images: http://www.blogoncherry.com/2011/08/25/10-terrorist-groups-in-the-world-according-to-america/.
[55] Terrorist images: http://www.nydailynews.com/new-york/terrorists-money-regional-cigarette-smugglers-ray-kelly-article-1.1346120.
[56] Terrorist images: http://www.topnews.in/law/pakistan-fomenting-terrorism-kashmir-india-255459.
[57] Terrorist images: http://www.ikhwanweb.com/article.php?id=17929.
[58] N.V. Botchkareva, M. Khlgatian, B.J. Longley, V.A. Botchkarev and B.A. Gilchrest, "SCF/c-kit signaling is required for cyclic regeneration of the hair pigmentation unit", *The Journal of the Federation of American Societies for Experimental Biology*, vol. 15, no. 3, pp. 645-659, 2001.
[59] P. Margot, "Commentary on the need for a research in forensic sciences", *UCLA Law Review*, vol. 58, no. 3, pp. 795-801, 2011.
[60] A.W.K. Kong and D. Zhang, "Competitive coding scheme for palmprint verification", *ICPR*, 2004, vol. 1, pp. 520-523.
[61] A. Nurhudatiana, A.W.K. Kong, K. Matinpour, D. Chon, L. Altieri, S.Y. Cho, and N. Craft, "The Individuality of Relatively Permanent Pigmented or Vascular Skin Marks (RPPVSM) in Independently and Uniformly Distributed Patterns", *TIFS*, vol. 8, no. 6, pp. 998-1012, 2013.
[62] V.A. Randall and N.V. Botchkareva, "The biology of hair growth", in Cosmetic Applications of Laser and Light-based system, G.S. Ahluwalia (ed.), William Andrew Inc. 2009.
[63] V.A. Randall and E.J.G. Ebling, "Seasonal changes in human hair growth", *Br. J. Dermatol*., vol. 124, pp. 146-151, 1991.
[64] Terrorist images: http://littlegreenfootballs.com/weblog/?entry=8589.
[65] D. Meuwly and R.G.F Veldhuis, "Forensic biometrics: from two communities to one discipline", Proceedings of International Conference of the Biometrics Special Interest Group, pp. 1-12, 2012.

Han Su received the M.Eng. and PhD degrees in computer science and technology from Harbin Engineering University, Harbin, China. From 2012 to 2013, she was a visiting scholar at the School of Computer Engineering, Nanyang Technological University, Singapore. Currently, she is an associate professor at the School of Computer Science, Sichuan Normal University, Chengdu, China. Her research interests include image processing, pattern recognition, and biometrics.

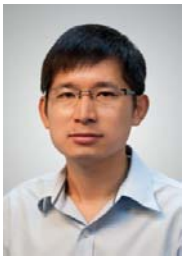

Adams Wai-Kin Kong received his PhD from the University of Waterloo, Canada. Currently, he is an associate professor at the Nanyang Technological University, Singapore. His research interests include biometrics, forensics, image processing, and pattern recognition.